Current Science International
Volume: 12 | Issue: 03| July – Sept.| 2023

EISSN:2706-7920 ISSN: 2077-4435
DOI: 10.36632/csi/2023.12.3.28
Journal homepage: www.curresweb.com
Pages: 398-410

Vacancy Defects in Carbon Nanotubes for Hydrogen Storage

M. A. Al-Khateeb[1,2], A. A. El-Barbary[3,4], M. A. Kamel[4] and Kh. M. Eid[4,5]

[1]Physics Department, Faculty of Education and Science, Taiz University, Taiz, Yemen.
[2]Medical Equipment Engineering Department, Faculty of Science and Engineering, Al -Rowad University, Taiz, Yemen.
[3]Physics Department, Faculty of Science, Jazan University, Jazan, Saudi Arabia.
[4]Physics Department, Faculty of Education, Ain Shams University, Cairo, Egypt.
[5]Department of Physics, College of Science and Arts, Qassim University, Albukayriyah 52725, Saudi Arabia.

Received: 10 June 2023 **Accepted:** 15 July 2023 **Published:** 30 July 2023

ABSTRACT

The hydrogen storage outside and inside carbon nanotube (CNT) has investigated at different positions using density functional theory (DFT) and applying 6-31g basis set. In addition, the effect of vacancy defects on hydrogen storage has been studied including mono-vacancy, di-vacancy and isolated monovacancy defects. The adsorption energy, HOMO (highest occupied molecular Orbital), LUMO (lowest unoccupied molecular orbital), energy gap, dipole moment and Mullikan Analysis are discussed. The results show that hydrogen molecule cannot be stored inside the CNT. However, the hydrogen molecule prefers to be stored outside the nanotubes. The most candidate CNT for hydrogen storge is found to be mono-vacancy defected CNT with hydrogen adsorption energy -3.8 eV.

Keywords: DFT, CNT, Hydrogen Storage, Vacancy defects, Adsorption Energy.

1. Introduction

Interest in hydrogen as a fuel has grown dramatically since 1990, and many advances in hydrogen production and utilization technologies have been made. Hydrogen provides more energy than either gasoline or natural gas on a weight basis. New approaches enabling more compact, lightweight, and energy efficient hydrogen storage are required for the wide-spread use of hydrogen powered vehicles to become a reality Elemental carbon in the sp2 hybridization can form a variety of amazing structures. Apart from the well-known graphite, carbon can build closed and open cages with honeycomb atomic arrangement. First such structure to be discovered was the C_{60} molecule by Kroto *et al.,* (1985). Although various carbon cages were studied, it was only in 1991, when Iijima, 1991 observed for the first-time tubular carbon structures. The nanotubes consisted of up to several tens of graphitic shells (so-called multi-walled carbon nanotubes (MWNTs)) with adjacent shell separation of 0.34 nm, diameters of 1 nm and large length/diameter ratio. Two years later, Iijima and Ichihashi, (1993) and Bethune *et al.,* (1993) synthesized single-walled carbon nanotubes (SWNTs). Nowadays, MWNTs and SWNTs are produced mainly by three techniques: arc-discharge, laser-ablation, and catalytic growth.

The nanotube is uniquely specified by the pair of integer numbers n, m or by its radius R $=Ch/2\pi$ and chiral angle θ which is the angle between Ch and the nearest zigzag of C–C bonds. All different tubes have angles θ between zero and 30°. Special tube types are the achiral tubes (tubes with mirror symmetry), armchair tubes (n, n) (θ = 30°) and zigzag tubes (n, 0) (θ = 0°). All other tubes are called chiral (m, n)(θ =120°) (Dresselhaus *et al.,* 1995).

Carbon nanotubes (CNTs) display superior mechanical properties and have many potential applications. One of them is the hydrogen storage because (i) carbon is a good adsorbent for gases;

Corresponding Author: M. A. Al-Khateeb, 1Physics Department, Faculty of Education and Science, Taiz University, Taiz, Yemen. Email: m_alkhateeb77@yahoo.com

and (ii) CNTs are microporous carbon macromolecules with high specific surface and have the potential to adsorb hydrogen in their nanostructures (Darkrim *et al.,* 2002).

Carbon materials such as graphene, graphene oxide (GO), single-wall and multi-wall carbon nanotubes. (SWCNT, MWCNT and purified), carbon nanofibers (CNF) and activated carbon (AC) have been dominated by the public about high storage capacities in carbon nanostructures (Mohan *et al.,* 2019; Froudakis, 2011 and Panella *et al.,* 2005). Therefore, theoretical studies on hydrogen storage for pure and defected nanomaterials are investigated (El-Barbary and Al-Khateeb, 2021; Al-Khateeb, and El-Barbary 2020, El-Barbary 2019, EL-Barbary 2016, EL-Barbary 2016, EL-Barbary 2016; EL-Barbary 2016; Hindi and EL-Barbary 2015; El-Barbary *et al.,* 2015; El-Barbary *et al.,* 2015; El-Barbary *et al.,* 2015; El-Barbary *et al.,* 2015; EL-Barbary 2018; El-Barbary *et al.,* 2014; El-Barbary *et al.,* 2013; El-Barbary *et al.,* 2003; El-Barbary 2015; El-Barbary 2015 and El-Barbary *et al.,* 2009).

Hydrogen storage in CNTs is considered as one of the essential challenges in developing a clean-burning hydrogen economy. Therefore, this topic is not only financially attractive but also it has important technological applications. The hydrogen storage capacities for CNTs have been reported by different laboratories (Yildirim *et al.,* 2005; Zhang *et al.,* 2004; Yang *et al.,* 2006; Kiyobayashi *et al.,* 2002; Tibbetts *et al.,* 2001; Zheng *et al.,* 2004; Anson *et al.,* 2006; Gundiah *et al.,* 2003; Zhao *et al.,* 2005 and Blackman *et al.,* 2006) differed by inconsistencies of test conditions as experimental conditions, methods of CNTs synthesis, pretreatment procedures, purification, and activation methods of CNTs. Most of the results testified that the storage capacity of CNTs for hydrogen is lower than 1 wt.% at ambient temperature (far from the practical applicability target of 6.5 wt.% at ambient temperature) but the capacity could be raised considerably to between 4 and 8 wt.% when decreasing the temperature of adsorption or modifying the CNTs or (Mohan *et al.,* 2019; Froudakis, 2011; Anson *et al.,* 2004; Shen *et al.,* 2004; Yurum *et al.,* 2009; Ioannatos and Verykios, 2010; Sharma and Kumar, 2016; Liu *et al.,* 2010; Mosquera *et al.,* 2014; Morel *et al.,* 2015; Spyrou *et al.,* 2013; Aboutabeli *et al.,* 2012; Jeing *et al.,* 2013; Dillon *et al.,* 1997; Deck and Vecchio 2006; Esconjauregui *et al.,* 2009; Liu *et al.,* 2010; Steiner *et al.,* 2009; Liang *et al.,* 2011; Zhen Zhou *et al.,* 2006; Hou *et al.,* 2011; Xue *et al.,* 2011; Shen *et al.,* 2012; He and Gao 2010; Kumar and Ando 2010; Han and Lee, 2004).

The obtained values have not yet reached the required standard by DOE (department of energy). Therefore, there is still a great challenge of finding a material that can store enough hydrogen under the standard conditions by DOE. Hence, the main aim of this work is to investigate the enhancement of vacancy defects on the hydrogen storage in CNTs. So, we concern to study the many factors as concentration of vacancy, distribution the vacancy within the tube and adsorption of H_2 inside and outside the tube to reach more specific conclusion.

2. Methods

In present study, we have carried out full geometry optimization with density functional theory (DFT) and 6-31G basis set. Many previous studies have been used DFT (Telling *et al.,* 2003; Suarez-Martinez *et al.,* 2007; Ewels *et al.,* 2003; EL-Barbary 2017; Shalabi *et al.,* 1998; Shalabi *et al.,* 1998). All calculations were carried out on a cluster of $C_{100}H_{20}$ using Gaussian 03W program (Savini *et al.,* 2007). The adsorption energy of hydrogen molecules on pristine CNT (Eads) according to the following expression (Shalabi *et al.,* 2001, Shalabi, 2001).

$$E_{ads} = E_{CNT\text{-}H2} - E_{CNT} - E_{H2}$$

where $E_{CNT\text{-}H2}$ is the energy of the optimized CNT-H_2 structure, E_{CNT} is the energy of an optimized CNT structure and E_{H2} is the energy of a hydrogen molecule. In addition, the electron density distribution, Mulliken analysis and molecular orbitals have been discussed.

3. Results and Discussion

3.1 Ab initio calculations of CNT

3.1.1 Ab initio calculations on pristine CNT:

The optimized structure of (5,5) CNT and its HOMO and LUMO are shown in Figure (1). Our calculated average bond length is 1.40 A° and average bond angle is 1200. HOMO represents the overlap between the adjacent carbon atoms, forming bond lengths are not perpendicular on the tube axis whereas LUMO which represents the overlap between the adjacent carbon atoms, forming bond lengths which are perpendicular on the tube axis. The values of HOMO, LUMO, energy band gap and dipole moment of pristine (5,5) CNT is presented in Table (1). Terminated carbon atoms are saturated by hydrogen atoms, resulting in opening band gap of (5,5) CNT to 5.6 eV. The dipole moment of perfect CNT is 0.0001 Debye. This value reflects that the reactivity (El-Barbary *et al.,* 2013 and El-Nahass et al.,2013) of the surface for pure CNT is too small.

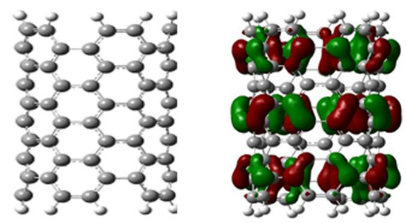

Fig. 1: a) The optimized structure of pristine C100H20 (5,5) CNT, b) itsHOMO and c) its LUMO. The gray and white atoms refer to carbon and hydrogen atom, respectively.

Table 1: The HOMO, LUMO, energy band gap and dipole moment of optimized $C_{100}H_{20}$ (5,5) CNT.

Structure	HOMO eV	LUMO eV	Eg eV	Dipole moment Debye
$C_{100}H_{20}$ (Perfect CNT)	-5.70	-0.10	5.60	0.0001

3.1.2. Ab initio calculations of mono-vacancy defected CNT

The optimized structure of mono-vacancy defected $C_{99}H_{20}$ (5,5) CNT and its HOMO and LUMO are shown in Figure (2). The structure of mono-vacancy defect is created by removing one carbon atom. Results in three dangling carbon atoms are formed, two of them are rebonded by 1.56Å and the third dangling carbon atom is kicked out of the surface of CNT. The values of HOMO, LUMO, energy band gap and dipole moment of mono-vacancy defected (5,5) CNT are represented in Table (2). From Figure (2), LUMO presents the mono-vacancy defect. It is found that there is no change. However, the reactivity of the surface is increased to 2.12 Debye.

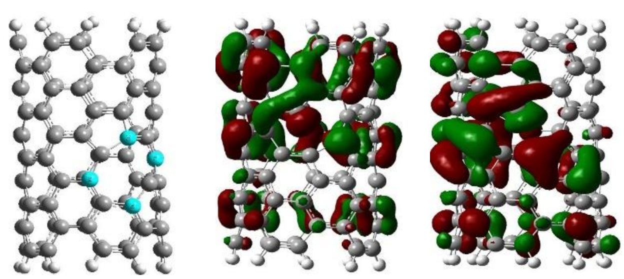

Fig. 2: a) The optimized structure of mono-vacancy defect of C99H20 (5,5) CNT and its, b) HOMO and c) LUMO. The gray and white atoms refer to carbon and hydrogen atoms, respectively. The blue atoms refer to the first neighbors carbon atoms to the defect.

Table 2: The HOMO, LUMO, energy band gap and dipole moment of optimized mono-vacancy defected $C_{99}H_{20}$ (5,5) CNT.

Structure	HOMO eV	LUMO eV	Eg eV	Dipole moment Debye
$C_{99}H_{20}$ Mono-vacancy CNT	-5.57	0.03	5.60	2.1205

3.1.3. Ab initio calculations of di-vacancy defected CNT

The optimized structure of di-vacancy defected $C_{98}H_{20}$ (5,5) CNT and its HOMO and LUMO are shown in Figure (3). The di-vacancy defect is created by removing two adjacent carbon atoms. Results in four dangling carbon atoms are formed, each two carbon atoms are rebonded by 1.53Å (EL-Barbary 2016). The HOMO, LUMO, energy band gap and dipole moment of di-vacancy defected (5,5) CNT are represented in Table (3). From the energy band gaps of pristine CNT, mono-vacancy, and di-vacancy CNT, it is found that the di-vacancy defect increases the energy band gap by 0.5 eV. The reactivity of the surface is 0.1209 Debye, higher than the pure CNT and less than the mono-vacancy defected of (5,5) CNT.

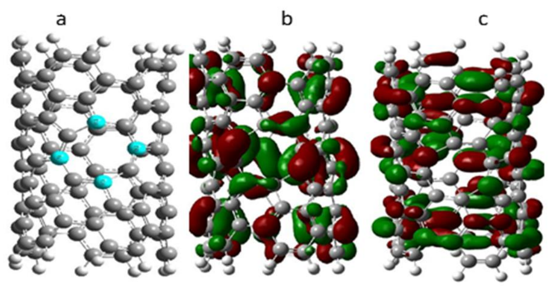

Fig. 3: a) The optimized structure of di-vacancy defected $C_{98}H_{20}$ (5,5) CNT b) its HOMO and c) its LUMO. The gray and white atoms refer to carbon and hydrogen atoms, respectively. The blue atoms refer to the first neighbors carbon atoms to the defect.

Table 3: The HOMO, LUMO, energy band gap and dipole moment of optimized di-vacancy defect of $C_{98}H_{20}$ (5,5) CNT

Structure	HOMO eV	LUMO eV	Eg eV	Dipole moment Debye
$C_{98}H_{20}$ di-vacancy CNT	-5.92	0.18	6.1	0.1209

3.1.4 Ab initio calculations of isolated mono-vacancies defectd CNT

The isolated mono-vacancy optimized structures of $C_{98}H_{20}$ (5,5) CNT and its HOMO and LUMO are shown in Figure (4). The isolated mono-vacancy defect is created by removing two separated carbon atoms, from different sites of CNT as shown in Figure (4). Results in three dangling carbon atoms are formed in each site, as mentioned in mono-vacancy defect. Therefore, two pentagons are formed, and two carbon atoms are kicked out of the CNT surface. The two pentagons are formed through bond length of 1.58 Å (13). The HOMO, LUMO, energy band gap and dipole moment of mono-vacancy (5,5) CNT are represented in Table (4). The reactivity of the surface is 2.172 Debye, like mono-vacancy defect. The values of energy band gaps, 5.6 eV, are like the pristine CNT and mono-vacancy CNT. This can be explained in terms of geometrical structures and distortion, i.e. the tube distortion of mono vacancy structure is quite negligible comparing with distortion of divacancy structure. Hence, only the HOMO and LUMO energies are changed while the band gap (the energy difference between HOMO and LUMO) does not change.

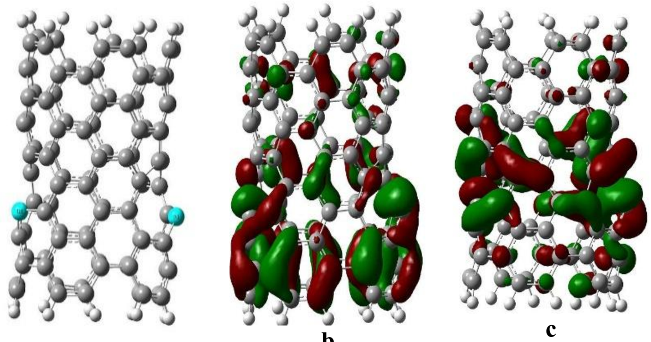

Fig. 4: a) The optimized structure of isolated mono-vacancy defected $C_{98}H_{20}$ (5,5) CNT , b) its HOMO and c) its LUMO. The gray and white atoms refer to carbon and hydrogen atoms, respectively. The blue atoms refer to the first neighbors carbon atoms to the defect.

Table 4: The HOMO, LUMO, energy band gap and dipole moment of optimized isolated mono-vacancy defect of $C_{98}H_{20}$ (5,5) CNT.

Structure	HOMO eV	LUMO eV	Eg eV	Dipole moment Debye
$C_{98}H_{20}$ Isolated mono-vacancy CNT	-6.1	-0.5	5.6	2.1720

3.2 Ab initio calculations of hydrogened CNT

3.2.1 Adsorption of H2 molecules inside the pristine CNT

The different adsorption configurations of a single hydrogen molecule in $C_{100}H_{20}$ (5,5) CNT are shown in Figure (5) and are calculated in Table (5). Symbols A, B, C and D present the four different structures of H_2 inside the pristine CNT, perpendicular, with 45° angle and parallel to the tube axis, respectively. The adsorption energy is endothermic (the required energy to push H_2 inside the tube) and is in the range of ~30meV, in good agreement with previous theoretical work 34.3 meV (Zhen Zhou *et al.,* 2006). Also, it is noticed that the energy band gap of pristine (5,5) CNT is not affected by H_2 molecule.

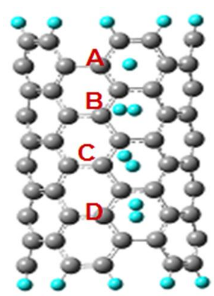

Fig. 5: Four different configurations of a single hydrogen molecule inside C100H20 (5,5) CNT. The gray and blue atoms refer to carbon and hydrogen atoms, respectively.

Table 5: The adsorption energies, HOMOs, LUMOs and energy band gaps of optimized structures of $H_2C_{100}H_{20}$ (5,5) CNT

Structure	E_{ads} meV	HOMO eV	LUMO eV	Eg eV
$H_2C_{100}H_{20}$ (5,5) (A)	38.19	-5.7	-0.1	5.6
$H_2C_{100}H_{20}$ (5,5) (B)	34.55	-5.7	-0.1	5.6
$H_2C_{100}H_{20}$ (5,5) (C)	30.60	-5.7	-0.1	5.6
$H_2C_{100}H_{20}$ (5,5) (D)	32.68	-5.7	-0.1	5.6

3.2.2 Adsorption of H_2 molecules inside vacancy defected CNT

The adsorption configurations of H2 for mono-vacancy defected H2C99H20, di-vacancy defected $H_2C_98H_20$ and isolated mono-vacancy defected $H_2C_98H_20$ of (5,5) CNT are shown in Figure

EISSN: 2706-7920 ISSN: 2077-4435 **DOI: 10.36632/csi/2023.12.3.28**

(6). From Table (6), the values of adsorption energies are larger than the adsorption energy of pristine CNT (the average adsorption energy of pristine CNT is ≅ 34 meV), indicating that the vacancy defects (mono-, di-, isolated mono- vacancies) do not enhance the hydrogen storage inside the (5,5) CNT. Also, the storage of H2 inside the (5,5) CNT does not change the energy band gaps of vacancy defects. To conclude, it is noticed that the energy band gap of pristine (5,5) CNT and vacancy defects is not affected by H2 molecule. This can explain because there is no any bonding between the H2 molecules and CNT when it is absorbed inside the tube, ending without any distortion within the tube and hence the effect of H2 molecules in the band gap is negligible. However, due to the concentration of vacancies in isolated mono-vacancies is twice the concentration in mono-vacancy, therefore, the adsorption energy for isolated mono-vacancies is higher than the mono-vacancy.

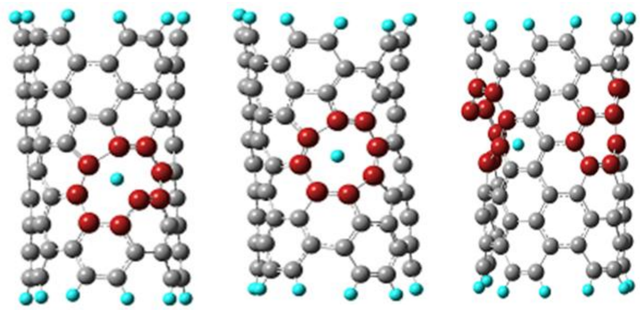

Fig. 6: Optimized structures of H_2 molecule inside a) mono-vacancy defected $H_2C_{99}H_{20}$ (5,5) CNT , b) di-vacancy defected $H_2C_{98}H_{20}$ (5,5) CNT and c) isolated mono-vacancy defected $H_2C_{98}H_{20}$ (5,5) CNT. The gray and blue atoms refer to carbon and hydrogen atoms, respectively. The red atoms refer to the first neighbors carbon atoms to the defect.

Table 6: The adsorption energies, HOMOs, LUMOs and energy band gaps of optimized structures of vacancy (5,5) defected CNT

Structure	E_{ads} meV	HOMO eV	LUMO eV	Eg eV
Mono-vacancy	51.74	-6.1	-0.5	5.6
Di-vacancy	62.83	-5.9	0.2	6.1
Isolated mono-vacancies	94.53	-6.1	-0.5	5.6

3.3 Ab initio calculations of hydrogen storage outside CNT

3.3.1 Adsorption of H_2 molecules outside the pristine CNT

Two different adsorption configurations of a single hydrogen molecule on the wall of $C_{100}H_{20}$ (5,5) CNT are shown in Figure (7). The adsorption energies and energy band gaps are calculated and given in Table (7). Symbols A and B are represented the two structures of H_2 adsorption outside the pristine CNT: when the center of bond length for H_2 is on the top of carbon atom and when each hydrogen atom is on the top of one carbon atom, respectively. The adsorption energy is endothermic and in the range of ~ 2eV, larger than the adsorption energy inside (5,5) CNT (30.60 meV). Also, it is noticed that the energy band gap is increased to 6.1 eV, comparing with the pristine (5,5) CNT of 5.6 eV.

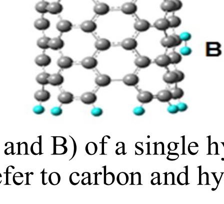

Fig. 7: Two different configurations (A and B) of a single hydrogen molecule outside $C_{100}H_{20}$ (5,5) CNT. The gray and blue atoms refer to carbon and hydrogen atoms, respectively.

EISSN: 2706-7920 ISSN: 2077-4435 **DOI: 10.36632/csi/2023.12.3.28**

Table 7: The adsorption energies, HOMOs, LUMOs and energy band gaps of optimized structures of $H_2C_{100}H_{20}$ (5,5) CNT

Structure	E_{ads} eV	LUMO eV	HOMO eV	Eg meV
A (B)	2.1	-5.9	0.2	6.1

3.3.2 Adsorption of H_2 molecules outside mono-vacancy defected (5,5) CNT

There are two different adsorption configurations of a single hydrogen molecule outside the wall of mono-vacancy defect of $C_{99}H_{20}$ (5,5) CNT, see Figure (8). The adsorption energies and energy band gaps are calculated and given in Table (8). a and b are represented the two structures of H_2 outside the mono-vacancy defect of (5,5) CNT: when the H_2 is on the top of the dangling carbon atom, and when it is adsorbed far from the mono-vacancy defect, respectively. The adsorption energy is exothermic (the energy released from adsorption of H_2 outside CNT) for the structure (a) and endothermic for structure (b). This means that the mono-vacancy defect enhances the hydrogen storage when the H_2 adsorbed around the defect.

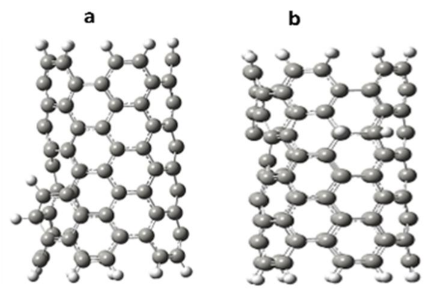

Fig. 8: a) and b) are two different configurations of a single hydrogen molecule outside mono-vacancy defected $H_2C_{99}H_{20}$ (5,5) CNT. The gray and white atoms refer to carbon and hydrogen atoms, respectively.

Table 8: The adsorption energies, HOMOs, LUMOs and energy band gaps of optimized structures of $H_2C_{99}H_{20}$ (5,5) CNT.

Structure	E_{ads} eV	HOMO eV	LUMO eV	Eg eV
mono- vacancy (a)	-3.79	**-5.7**	**-0.1**	5.6
mono -vacancy (b)	0.14	**-5.7**	**-0.1**	5.6

3.3.3 Adsorption of H_2 molecules outside di-vacancy defected (5,5) CNT

There are three different adsorption configurations of a single hydrogen molecule outside the wall of di-vacancy defect of $C_{98}H_{20}$ (5,5) CNT, see Figure (9). The adsorption energies and energy band gaps are calculated and given in Table (9). Symbols a, b and c are represented the three structures of H_2 outside the di-vacancy defect of (5,5) CNT: when one atom of H_2 molecule is above one carbon atom of pentagon ring and the other hydrogen atom is above one carbon atom of the adjacent hexagon ring, when the center of bond length of H_2 molecule is above one carbon atom of pentagon ring, and when the H_2 molecule is adsorbed far away from the di-vacancy defect, respectively. The adsorption energy is exothermic for the structures (a and b) and endothermic for structure (c). This means that the di-vacancy defect enhances the hydrogen storage when the H_2 adsorbed above the pentagon ring.

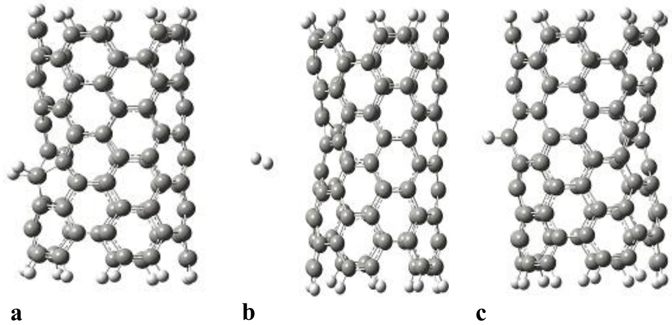

Fig. 9: a), b) and c) are three different configurations of a single hydrogen molecule outside di-vacancy defected $H_2C_{98}H_{20}$ (5,5) CNT. The gray and white atoms refer to carbon and hydrogen atoms, respectively.

Table 9: The adsorption energies, HOMOs, LUMOs and energy band gaps of optimized structures of $H_2C_{98}H_{20}$ di-vacancy defcetd (5,5) CNT

Structure	E_{ads} eV	HOMO eV	LUMO eV	Eg eV
Di- vacancy (a)	-1.227	-5.95	0.25	6.2
Di- vacancy (b)	-0.007	-5.92	0.08	6.0
Di- vacancy (c)	0.534	-5.59	0.01	5.6

3.3.4 Adsorption of H_2 molecules outside isolated mono-vacancy defected (5,5) CNT

There are three different adsorption configurations of a single hydrogen molecule outside the wall of isolated mono-vacancy defected $C_{98}H_{20}$ (5,5) CNT, see Figure (10). The adsorption energies and energy band gaps are calculated and given in Table (10). a, b and c are presented the three structures of H_2 outside the isolated mono-vacancy defected (5,5) CNT, when one atom of the H_2 molecule is above the dangling carbon atom of pentagon ring and the other hydrogen atom is above one carbon atom of the adjacent hexagon ring, when the center of bond length of H_2 molecule is on the top of the dangling carbon atom, and when the H_2 molecule is adsorbed far away from the isolated mono-vacancy defect, respectively. The adsorption energy is exothermic for all three structures of isolated mono-vacancy defects; however, the more negative chemisorbed energy is for structure (b).

One can conclude that the adsorption energies for all types of vacancy defects (mono-vacancy, isolated mono-vacancies and di-vacancies) are enhanced by adsorptions H_2 molecule outside the wall rather than inside the wall of CNTs. The obtained results could be explained due to new bonds created between H2 molecules and vacancy defects when the adsorption is outside the wall, results in changing the geometric structures and the obtained energy gaps and adsorption energy.

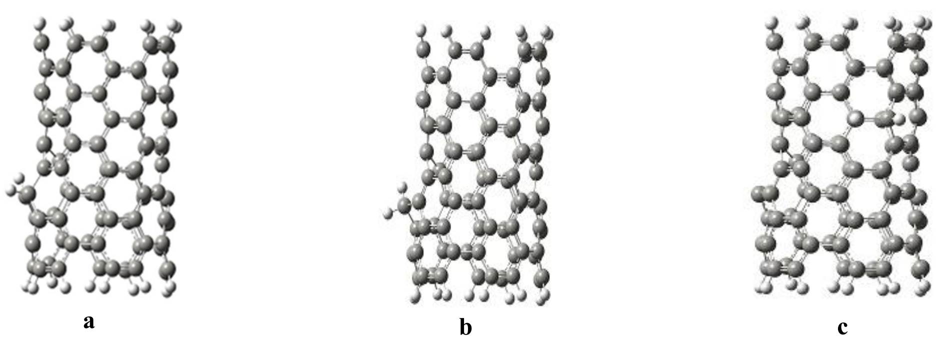

Fig. 10: a), b) and c) are three different configurations of a single hydrogen molecule outside isolated mono-vacancy defected $H_2C_{98}H_{20}$ (5,5) CNT. The gray and white atoms refer to carbon and hydrogen atoms, respectively.

Table 10: The adsorption energies, HOMOs, LUMOs and energy band gaps of optimized structures of $H_2C_{98}H_{20}$ (Isolated mono-vacancy) (5,5) CNT

Structure	E_{ads} eV	HOMO eV	LUMO eV	Eg eV
Isolated mono- vacancy (a)	-0.759	-5.29	-0.89	4.4
Isolated mono- vacancy (b)	-3.814	-5.93	-0.23	5.7
Isolated mono -vacancy (c)	-0.532	-6.32	-0.12	6.2

3.4. Mulliken analysis and Molecular orbitals

We present the Mulliken analysis and Molecular orbitals for selected sites of H_2 adsorption that they possess the best adsorption energies. Figure (11(a, b)) shows the Mulliken analysis for H_2 adsorption outside the mono- vacancy and isolated mono-vacancy defected (5,5) CNT. The charge transfer is localized around the vacancy defect and there is no charge transfer far from the vacancy defect sites. Figure (12(a, b, c, d)) show the HOMO and LUMO for mono-vacancy and isolated mono-vacancy defected (5,5) CNT. There is charge overlap between the adjacent atoms around the vacancy defect, leading to the reduction of the adsorption energy of H_2 outside (5,5) CNT, agrees well with previous theoretical work (Zhen Zhou *et al.,* 2006).

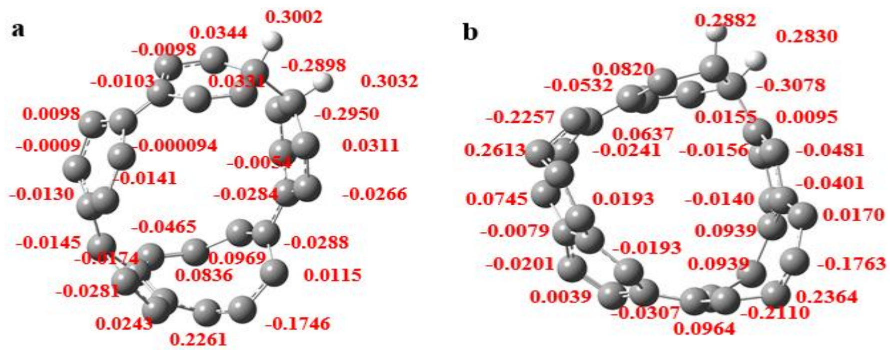

Fig. 11: Mullikan analysis for H_2 adsorption outside the (a) mono- vacancy and (b) isolated mono-vacancy defected (5,5) CNT. The gray atoms refer to carbon atoms.

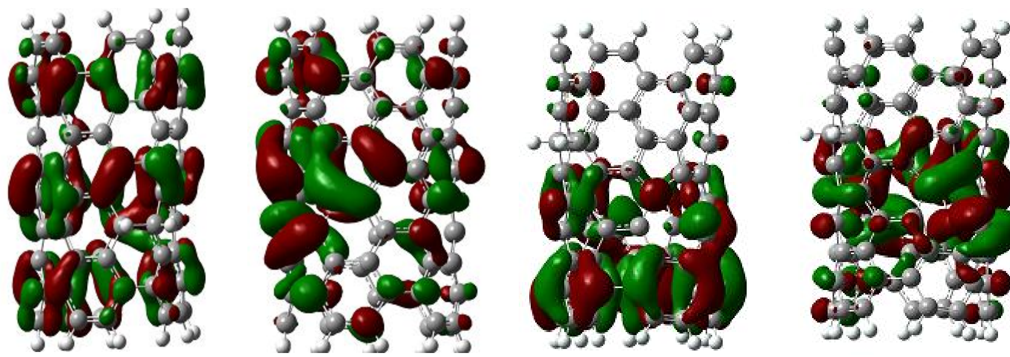

a b c d

Fig. 12: Molecular orbitals of mono-vacancy (a) HOMO and (b) LUMO, and for isolated mono-vacancy (c) HOMO and (d) LUMO.

4. Conclusion

We have studied the energy band gaps for pristine and defected (5,5) CNTs at different concentrations and at different distributions inside and outside the CNTS. It is found that the adsorption of H_2 outside the pristine and defected (5,5) CNT is physisorption energy. However, most of the adsorption of H_2 outside the defected (5,5) CNT is chemisorption energy. The more negative chemisorption energy is -3.8 eV for the adsorbed H_2 molecule outside the mono-vacancy (or isolated mono-vacancy) defect of (5,5) CNT. Finally, one can conclude that the hydrogen storage in CNT is enhanced by the monovacancy defects more than divacancies when the H2 adsorbed outside the tube.

5. References

Aboutabeli, S.H., S. Aminorroaya-Yamini, I. Nevirkovets, K. Konstantinov, and H.K. Liu, 2012. Enhanced Hydrogen storage in graphene oxide-MWCNTs composite at room temperature, Adv. Energy Mater, 2: 1439–1446.

Al-Khateeb, M.A., and A.A. El-Barbary, 2020. Hydrogen Adsorption Mechanism of SiC Nanocones, Graphene, 9: 1-12.

Anson, A., E. Lafuente, E. Urriolabeitia, R. Navarro, A.M. Benito, W.K. Maser, *et al.,* 2006. Hydrogen capacity of palladium-loaded carbon materials. J. Phys. Chem. B., 110: 6643–8.

Anson, A., M.A. Callejas A.M. Benito, W.K. Maser, M.T. Izquierdo, B. Rubio, *et al.,* 2004. Hydrogen adsorption studies on single wall carbon nanotubes. Carbon, 42: 1243–8.

Bethune, D.S., C.H. Kiang, M.S. de Vries, G. Gorman, R. Savoy, J. Vazquez, and R. Beyers, 1993. Cobalt-catalysed growth of carbon nanotubes with single-atomic-layer waiis, Nature (London) 363: 605.

Blackman, J.M., J.W. Patrick, and C.E. Snape, 2006. An accurate volumetric differential pressure method for the determination of hydrogen storage capacity at high pressures in carbon materials. Carbon, 44: 918–27.

Darkrim, F.L., P. Malbrunot, and G.P. Tartaglia, 2002. Review of hydrogen storage by adsorption in carbon nanotubes, Int. J. Hydrogen Energy, 27 (2):193.

Deck, C.P., and K. Vecchio, 2006. Prediction of carbon nanotube growth success by the analysis of carbon–catalyst binary phase diagrams, Carbon, 44: 267–275.

Dillon, A.C., K.M. Jones, T.A. Bekkedahl, C.H. Kiang, D.S. Bethune, and M.J. Heben, 1997. Storage of hydrogen in single-walled carbon nanotubes, Nature, 386: 377–379.

Dresselhaus, M.S., G. Dresselhaus, and R. Saito, 1995. Physics of carbon nanotubes, Carbon, 33: 883.

El-Barbary, A.A., 2015. ^{1}H and ^{13}C NMR Chemical Shift Investigations of Hydrogenated Small Fullerene Cages C_n, C_nH, C_nH_n and C_nH_{n+1}: n=20, 40, 58, 60., Journal of Molecular Structure, 1097: 76-86.

El-Barbary, A.A., 2015. The Surface Reactivity and Electronic Properties of Small Hydrogenation Fullerene Cages., Journal of Surface Engineered Materials and Advanced Technology, 5:162-168.

EL-Barbary, A.A., 2016. Hydrogenated fullerenes dimer, peanut and capsule: An atomic comparison., Applied Surface Science, 369: 50-57.

EL-Barbary, A.A., 2016. Hydrogenated fullerenes in space: FT-IR spectra analysis., AIP Conference Proceedings, 1742.

EL-Barbary, A.A., 2016. Hydrogenation Mechanism of Small Fullerene Cages. International Journal of Hydrogen Energy, 41: 375-383.

EL-Barbary, A.A., 2016. Potential Energy of H2 inside the C116 Fullerene Dimerization: An Atomic Analysis., Journal of Molecular Structure, 1112: 9-13.

EL-Barbary, A.A., 2017. New Insights into Canted Spiro Carbon Interstitial in Graphite., Applied Surface Science, 426: 238-243.

EL-Barbary, A.A., 2018. Vacancy cluster in graphite: Migration energy and aggregation mechanism, Vacancy Cluster in Graphite: AIP Conference Proceedings, 1976.

El-Barbary, A.A., 2019. Hydrogen storage on cross stacking nanocones., International Journal of Hydrogen Energy, 44: 20099-20109.

El-Barbary, A.A., and M.A. Al-Khateeb, 2021. DFT Study of Se-doped Nanocones as Highly Efficient Hydrogen Storage Carrier, Graphene 10 (4): 49-60.

El-Barbary, A.A., G.H. Ismail, and A. Babaier, 2013. Theoretical Study of Adsorbing CO, CO_2, NO and NO_2 on Carbon Nanotubes., Journal of Surface Engineered Materials and Advanced Technology, 3: 287-294.

El-Barbary, A.A., H.I. Lebda, and M.A. Kamel, 2009. The high conductivity of defect fullerene C_{40} cage., Computational Materials Science, 46: 128-132.

El-Barbary, A.A., K.M. Eid, M.A. Kamel, H.O. Taha, and G.H. Ismail, 2015. Adsorption of CO, CO_2, NO and NO_2 on Boron Nitride Nanotubes: DFT Study., Journal of Surface Engineered Materials and Advanced Technology, 5: 154-161.

El-Barbary, A.A., K.M. Eid, M.A. Kamel, H.O. Taha, and G.H. Ismail, 2015. Adsorption of CO, CO_2, NO and NO_2 on Carbon Boron Nitride Hetero Junction: DFT Study., Journal of Surface

Engineered Materials and Advanced Technology, 5: 169-176.

El-Barbary, A.A., K.M. Eid, M.A. Kamel, H.O. Taha, and G.H. Ismail, 2014. Effect of Tubular Chiralities and Diameters of Single Carbon Nanotubes on Gas Sensing Behavior: A DFT Analysis., Journal of Surface Engineered Materials and Advanced Technology, 4: 66-74.

El-Barbary, A.A., M.A. Kamel, K.M. Eid, H.O. Taha, and M.M. Hassan, 2015. Mono-Vacancy and B-Doped Defects in Carbon Heterojunction Nanodevices., Graphene, 4: 84-90.

El-Barbary, A.A., M.A. Kamel, K.M. Eid, H.O. Taha, R.A. Mohamed, and M.A. Al-Khateeb, 2015. The Surface Reactivity of Pure and Monohydrogenated Nanocones Formed from Graphene Sheets.,Graphene, 45: 75-83.

El-Barbary, A.A., M.M. El-Nahass, M.A. Kamel, and M.A.M. El-Mans., 2013. On the Spectroscopic Analyses of Thioindigo Dye. Spectrochimica Acta Part A: Molecular and Biomolecular Spectroscopy, 113:332-336.

El-Barbary, A.A., R.H. Telling, C.P. Ewels, and M.I. Heggie, 2003. Structure and energetics of the vacancy in graphite., Physical Review B, 68:144107.

El-Nahass, M.M., M.A. Kamel, A.A. El-Barbary, M.A.M. El-Mansy, and M. Ibrahim, 2013. FT-IR spectroscopic analyses of 4-hydroxy-1-methyl-3-[2-nitro-2-oxoacetyl-2(^{1}H)quinolinone (HMNOQ)., Spectrochimica Acta Part A: Molecular and Biomolecular Spectroscopy, 113: 332-336.

Esconjauregui, S., C.M. Whelan, and K. Maex, 2009. The reasons why metals catalyze the nucleation and growth of carbon nanotubes and other carbon nanomorphologies, Carbon, 47: 659–669.

Ewels, C.P., R.H. Telling, A.A. El-Barbary, and M.I. Heggie,. Metastable Frenkel Pair Defect in Graphite: Source of Wigner Energy?., Physical Review Letters, 91:025505.

Frisch, M.J., G.W. Trucks, H.B. Schlegel, G.E. Scuseria, et al., 2004. Gaussian, Inc., Wallingford CT.

Froudakis, G.E., 2011. Hydrogen storage in nanotubes and nanostructures. Mater, Today Off. 14: 324–328

Gundiah, G., A. Govindaraj, N. Rajalakshmi, and K.S. Dhathathreyan, 2003. C.N.R. Rao, Hydrogen storage in carbon nanotubes and related materials. J. Mater Chem.,13:209–13.

Han, S.S., and H.M. Lee, 2004. Growth of Boron Nitride Nanotubes Having Large Surface Area Using Mechanothermal Process, carbon, 42: 2169.

He, H.K., and C. Gao, 2010. Supraparamagnetic, conductive, and processable multifunctional graphene nanosheets coated with high-density Fe3O4 nanoparticles, ACS Appl. Mater. Interfaces, 2: 3201–3210.

Hindi, A.A., and A.A. EL-Barbary, 2015. Hydrogen Storage on Halogenated C_{40} Cage: An Intermediate between Physisorption and Chemisorptions., Journal of Molecular Structure, 1080: 169-175.

Hou, C.Y., Q.H. Zhang, M.F. Zhu, Y.G. Li, and H.Z. Wang, 2011. One-step synthesis of magnetically-functionalized reduced graphite sheets and their use in hydrogels, Carbon, 49: 47–53.

Iijima S., 1991. Helical microtubules of graphitic carbon, Nature (London) 354: 56.

Iijima, S., and T. Ichihashi, 1993. Single-shell carbon nanotubes of 1-nm diameter, Nature (London) 363: 603.

Ioannatos, G.E., and X.E. Verykios, 2010. H2 storage on single- and multi-walled carbon nanotubes. Int. J. Hydrogen Energy, 35: 622–8.

Jeing, H., Y. Feng, M. Chen, and Y. Wang, 2013. Synthesis and hydrogen-storage performance of interpenetrated MOF-5/MWCNTs hybrid composite with high mesoporosity, Int. J. Hydrogen Energy, 38:10950–10955.

Kiyobayashi, T., H.T. Takeshita, H. Tanaka, N. Takeichi, A. Zuttel, and L. Schlapbach, 2002. Hydrogen adsorption in carbonaceous materials: how to determine the storage capacity accurately. J. Alloys Compd. 330–332, 666–9.

Kroto, H.W., J.R. Heath, S.C.O. Brien, R.F. Curl and R.E. Smalley, 1985. C_{60}: Buckminsterfullerene, Nature 318: 162

Kumar, M., and Y. Ando, 2010. Chemical vapor deposition of carbon nanotubes: a review on growth mechanism and mass production, J. Nanosci. Nanotechnol, 10: 3739–3758.

Liang, J.J., Y. Huang, J. Oh, M. Kozlov, D. Sui, S.L. Fang, R.H. Baughman, Y.F. Ma, and Y.S. Chen, 2011. Electromechanical actuators based on graphene and graphene/Fe_3O_4 hybrid, Adv. Funct. Mater, 21: 3778–3784.

Liu, C., Y. Chen, C.-Z. Wu, S.-T. Xu, and H.-M. Cheng, 2010. Hydrogen storage in carbon revisited, Carbon, 48: 452–455.

Liu, H., D. Tagaki, S. Chiashi, T. Chokan, and Y. Homma, 2010. Investigation of catalytic properties of Al2O3 particles in the growth of single-walled carbon nanotubes, J. Nanosci. Nanotechnol, 10: 4068–4073.

Mohan, V.K., E.A. Sharma, V. Kumar, and V. Gayathri, 2019. Hydrogen storage in carbon materials–A review, Energy Storage 1: 1–26.

Morel, M., E. Mosquera, D.E. Diaz-Droguett, N. Carvajal, M. Roble, V. Rojas, and R. Espinoza-Gonzalez, 2015. Mineral magnetite as precursor in the synthesis of MultiWalled Carbon Nanotubes and their capabilities of hydrogen adsorption, Int. J. Hydrogen Energy, 40: 15540–15548.

Mosquera, E., D.E. Diaz-Droguett, N. Carvajal, M. Roble, M. Morel, and R. Espinoza, 2014. Characterization and hydrogen storage in multi-walled carbon nanotubes grown by aerosol-assisted CVD method, Diam. Relat. Mater, 43: 66–71.

Panella, B., M. Hirscher, and R. Siegmar, 2005. Hydrogen adsorption in different carbon nanostructures, Carbon 43: 2209–2214.

Savini, G., A.A. EL-Barbary, M.I. Heggie, and S. Őberg, 2007. Partial dislocations under forward bias in SiC., Materials Science Forum, 556: 279-282.

Shalabi, A.S., A.M. El-Mahdy, Kh.M. Eid, M.A. Kamel, and A.A. El-Barbary, 2001. U2 center, adsorption, coadsorption and epitaxial growth of Cu, Ag and Au on LiH(0 0 1) surface: DFT calculations., Surface Science, 488:164-176.

Shalabi, A.S., Kh.M. Eid, M.A. Kamel, and A.A. El-Barbary, 1998. Comparative Study of Errors in HeH¯ Interaction Energy Calculations., International Journal of Quantum Chemistry, 68: 329.

Shalabi, A.S., Kh.M. Eid, M.A. Kamel, and A.A. El-Barbary, 1998. Potential Energy Curves of H and H ¯ Interactions with He., Physics Letters A, 239:87-93.

Shalabi, A.S., Kh.M. Eid, A.M. El-Mahdy, M.A. Kamel and A. A El-Barbary, 2001. Bulk dislocation-U defect interaction, surface excitons and adsorptivity of atomic H on dislocated surfaces of Lith crystal: ab initio calculations., Modelling Simul. Mater. Sci. Eng, 9:67.

Sharma, V.K., and E.A. Kumar, 2016. Metal hydrides for energy applications-classification, PCI characterization and simulation, Int. J. Energy Res., 14: 901–923

Shen, J.H., Y.H. Zhu, K.F. Zhou, X.L. Yang, and C.Z. Li, 2012. Tailored anisotropic magnetic conductive film assembled from graphene-encapsulated multifunctional magnetic composite microspheres, J. Mater. Chem., 22: 545–550.

Shen, K., H. Xu, Y. Jiang, and T. Pietraß, 2004.The role of carbon nanotube structure in purification and hydrogen adsorption. Carbon, 42: 2315–22.

Spyrou, K., D. Gournis, and P. Rudolfa, 2013. Hydrogen storage in graphene-based materials: efforts towards enhanced hydrogen absorption, ECS J. Solid State Sci. Technol, 2: M3160–M3169.

Steiner, S.A., T.F. Baumann, B.C. Bayer, R. Blume, M.A. Worsley, W.J. MoberlyChan, E.L. Shaw, R. Schlogl, A.J. Hart, S. Hofmann, and B.L. Wardle, 2009. Nanoscale zirconia as a € nonmetallic catalyst for graphitization of carbon and growth of single- and multiwall carbon nanotubes, J. Am. Chem. Soc, 131:12144–12154.

Suarez-Martinez, A.A. EL-Barbary, G. Savini, and M.I. Heggie, 2007. First-principles simulations of boron diffusion in graphite., Physical Review Letters, 98, Article ID: 015501.

Telling, R.H., C.P. Ewels, A.A. El-Barbary, and M.I. Heggie, 2003. Wigner Defects Bridge the Graphite Gap., Nature Materials, 2: 333-337.

Tibbetts, G.G., G.P. Meisner, and C.H. Olk, 2001. Hydrogen storage capacity of carbon nanotubes, filaments, and vapor-grown fibers. Carbon, 39: 2291–301.

Xue, Y.H., H. Chen, D.S. Yu, S.Y. Wang, M. Yardeni, Q.B. Dai, M.M. Guo, Y. Liu, F. Lu, J. Qu, and L.M. Dai, 2011. Oxidizing metal ions with graphene oxide: the in situ formation of magnetic nanoparticles on self-reduced graphene sheets for multifunctional applications, Chem. Commun, 47: 11689–11691.

Yang, F.H., A.J. Lachawiec , and R.T. Yang, 2006. Adsorption of spillover hydrogen atoms on single-wall carbon nanotubes. J Phys Chem. B 10: 6236–44.

Yildirim, T., J. Iniguez, and S. Ciraci, 2005. Molecular and dissociative adsorption of multiple hydrogens on transition metal decorated C60. Phys. Rev. B., 72:153403.

Yurum, Y., A. Taralp, and T.N. Veziroglu, 2009. Storage of hydrogen in nanostructured carbon materials. Int. J. Hydrogen Energy, 34: 3784–98.

Zhang, C., X. Lu, and A. Gu, 2004. How to accurately determine the uptake of hydrogen in carbonaceous materials. Int J Hydrogen Energy 29:1271–6.

Zhao, Y., Y.H. Kim, A.C. Dillon, M.J. Heben, and S.B. Zhang, 2005. Hydrogen storage in novel organometallic buckyballs. Phys. Rev. Lett., 94:155504–7.

Zhen, Z., G. Xueping, Y. Jie, S. Deying, 2006. Doping effects of B and N on hydrogen adsorption in single-walled carbon nanotubes through density functional calculations, Carbon, 44:939.

Zheng, Q., A. Gu, X. Lu, and W. Lin, 2004. Temperature-dependent state of hydrogen molecules within the nanopore of multi-walled carbon nanotubes. Int. J. Hydrogen Energy, 29:481–9.